SLAC-PUB-12271
January 2007

Relativistic effects on reflection X-ray spectra of AGN

Khee-Gan Lee [A,B,C], *Steven V. Fuerst* [D], *Graziella Branduardi-Raymont* [A], *Kinwah Wu* [A,E], *and Oliver Crowley* [A,B]

[A] Mullard Space Science Laboratory, University College London, Holmbury St. Mary, Surrey RH5 6NT, United Kingdom

[B] Department of Physics & Astronomy, University College London, Gower Street, London WC1E 6BT, United Kingdom

[C] Department of Astrophysical Sciences, Princeton University, Princeton, NJ 08544, USA

[D] Kavli Institute for Particle Astrophysics and Cosmology, Stanford University, Stanford, CA 94309, USA

[E] Email: kw@mssl.ucl.ac.uk

Abstract: We have calculated the reflection component of the X-ray spectra of active galactic nuclei (AGN) and shown that they can be significantly modified by the relativistic motion of the accretion flow and various gravitational effects of the central black hole. The absorption edges in the reflection spectra suffer severe energy shifts and smearing, The degree of distortion depends on the system parameters, and the dependence is stronger for some parameters such as the inner radius of the accretion disk and the disk viewing inclination angles. The relativistic effects are significant and are observable. Improper treatment of the reflection component of the X-ray continuum in spectral fittings will give rise to spurious line-like features, which will mimic the fluorescent emission lines and mask the relativistic signatures of the lines.

Keywords: accretion, accretion disks — galaxies: active — X-rays: galaxies — black hole physics — relativity

1 Introduction

The power-law component in the keV X-ray spectra of active galactic nuclei (AGN) is believed to be produced by inverse-Compton scattering of low-energy photons from the accretion disk by energetic electrons in a hot corona above the disk (Thorne & Price 1975; Sunyaev & Titarchuk 1980; Pozdnyakov, Sobel & Sunyaev 1983). The scattered emission is nearly isotropic, thus a fraction of it emerges directly as the observed power-law component, and the rest of it is incident onto the accretion disk, where it is further reprocessed by the cooler disk atmosphere. The back irradiation leads to the formation of fluorescent lines (most prominently, the neutral Fe Kα line at 6.4 keV) and a Compton-reflection continuum (for an overview, see Reynolds & Nowak (2003)). These fluorescent lines are intrinsic narrow because of their small thermal widths, but they can be broadened by scattering, relativistic motions of accretion-disk flows and strong gravity of the black hole. They can also be modified by the line-of-sight materials through absorption and scattering. The fluorescent lines are powerful diagnostic of the inner AGN environments, and they have been studied intensively in the last few decades. (See e.g., Cunningham (1976); Fabian et al. (1989); Stellar (1990); Laor (1991); Fanton et al. (1997); Dabrowski et al. (1997); Pariev & Bromley (1998); Reynolds et al. (1999); Fuerst & Wu (2004); Fuerst (2005); Wu et al. (2006).) The Compton-reflection continuum, like the lines, can be modified by relativistic motion of the flows, gravity of the black hole, and line-of-sight absorption and scattering. It is also a useful diagnostic of AGN accretion. In spite of this, the relativistic reflection continuum component in the AGN spectrum has not been subject to a similar degree of attention as the fluorescent lines.

Here we present a systematical analysis of the effects of gravity and relativistic motion on the Compton-reflection spectra of AGN. We quantify the distortion of the spectral features and investigate their dependence on system parameters, such as the inner and outer radii of the accretion disk, viewing inclination angle, and spin of the black hole. We organize the paper as follows. §2 describes the formulation and the numerical algorithm that we use in the spectral calculations. §3 presents reflection spectra in various settings and illustrates how the spectral features vary with system parameters. §4 discusses the astrophysical implications and applications.

2 Spectral calculations

We consider azimuthal symmetric, geometrically thin accretion disks in Keplerian rotation. The reflection emission originate from the disk surface layer. It is anisotropic and is subject to limb effects. We ignore any line-of-sight emission and extinction not directly related to the accretion disk. The photons are gravitationally lensed and their energies are relativistically shifted. The photon trajectories (the light rays) are de-

Work supported in part by the US Department of Energy contract DE-AC02-76SF00515

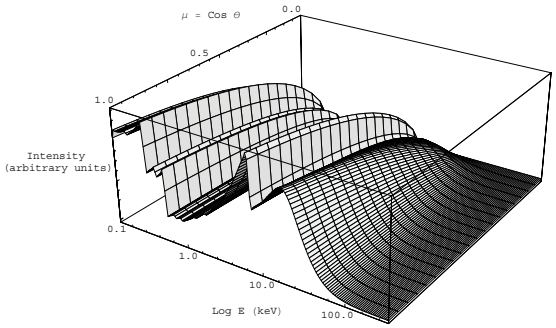

Figure 1: A surface plot showing the angle-dependence of reflection rest-frame spectra, generated by PEXRAV in XSPEC. The photon pitching angle θ is specified by the variable μ ($\equiv \cos\theta$). The metal abundance is set to be solar. All other parameters are fixed. The intensity is on a linear scale and in arbitrary units. The carbon (C), Oxygen (O) and Iron (Fe) edges (at 0.29, 0.54 and 7.1 keV respectvely) are clearly visible.

termined by the geodesic equation for the space-time specified by the black hole. The total spectrum of the accretion disk is the direct sum of contributions of all emitting disk surface elements. The spectral calculations consist of three parts: (1) generation of local reflection rest-frame spectra at different viewing angles, (2) calculation of local energy shifts and pitching angles of emerging photons that can reach the distant observer for each surface element on the accretion disk, and (3) convolution of the reflection rest-frame spectra, and the energy shifts and pitching angles of the photons for all disk surface elements.

2.1 Reflection rest-frame spectra

The main features in the reflection spectra are the continuum and edges. The most prominent edges are the carbon (C) edge at 0.288 keV, oxygen (O) edge at 0.538 keV and iron (Fe) edge at 7.117 keV. The reflection emission is anisotropic. The depths of edges and the strength of the underlying continuum all vary with the viewing inclination angle. We consider the prescription given in Magdziarz & Zdziarski (1995) (hereafter MZ95) to model the local reflection rest-frame spectra. The MZ95 spectra are closed-form approximations to Monte Carlo calculations of the reflected photons' Green's functions. They are generated using the PEXRAV routine in the XSPEC package (Schafer, Heberl & Arnaud 1991). Figure 1 shows the reflection rest-frame spectra for a full range of μ ($\equiv \cos\theta$, where θ is the pitching angle of the photons). The variations of the edges are the continuum with μ are clearly visible.

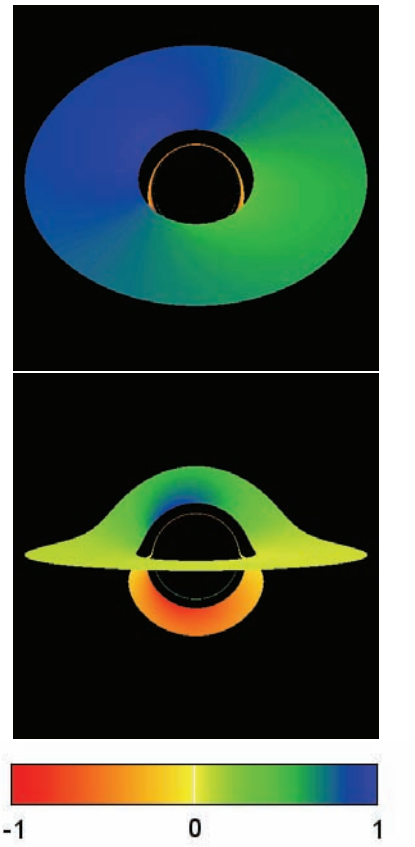

Figure 2: The distribution of μ on an accretion disk around a Schwarzschild black hole, viewed at inclinations angles of 45° (top panel) and 85° (bottom panel). The inner and the outer disk radii are 6 and 20 $r_{\rm g}$ respectively, where $r_{\rm g} = GM/c^2$ is the gravitational radius, G is the gravitational constant, c is the speed of light, and M is the black-hole mass. The colour code bar indicates the value of μ, with positive values for photons emitted from the 'top' surface and negative valuses for photons emitted from the 'bottom' surface.

2.2 Energy shift and lensing of the disk emission

The energy shifts and the degree of boosting of the emission depend on the flow speeds of the material in the emitting surface element relative to the observer and on the gravitational potential difference between the emitter and the observer. The energy-shift factor is given by $g = E_{\rm o}/E_{\rm e}$, where $E_{\rm o}$ and $E_{\rm e}$ are the observed and emitted energies of the photons respectively. The photon flux at a local rest-frame on a disk surface and the photon flux measured by the observer differ by a multiplication factor of g^4, where the factor of g^3 takes account of intensity boost due to energy (frequency) shift, and an additional factor of g takes account of time dilation.

For each surface element photons of a specific pitching angle can reach the distant observer, and the rest

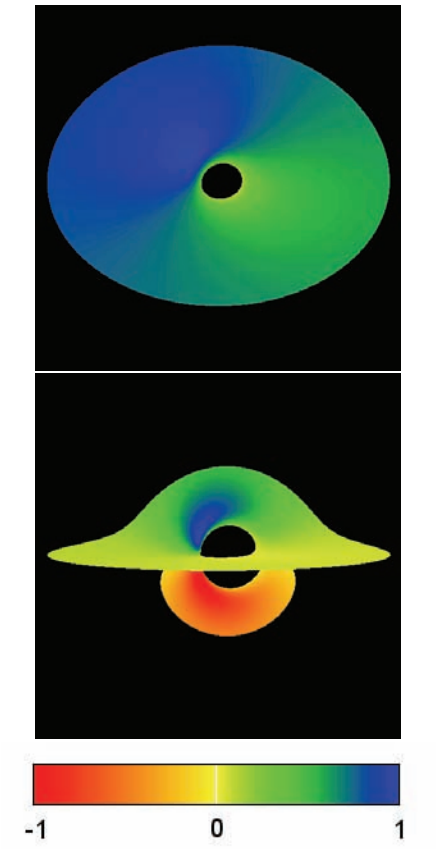

Figure 3: Same as Fig. 2 for rotating black holes with $a = 0.998$. The inner radius is set to be 1.23 $r_{\rm g}$; the other system parameters are the same as in the case of the Schwarzschild black hole.

photons emitted from the element will not be seen by the observer. Because of gravitational lensing, the pitching angles of these photons are not same as the viewing inclination angle of the accretion disk. They are also affected strongly by the local flow velocities and the rotation frame-dragging of the black hole. Combining all these effects make the pitching angle of the visible photons vary very significantly across the accretion disk.

We consider a backward ray-tracing algorithm and use the formulation given in Fuerst & Wu (2004) for the radiative transfer calculations. We first determine the energy shift factor g and and the cosine of the patch angle μ of the photons from for each surface element in the accretion disk and then generate disk images (projected in the sky-plane). The outputs of calculations for each set of accretion-disk and black-hole parameters are stored and will be used as inputs in the convolution calculations.

Figures 2 and 3 show distributions of the photon pitching angles in accretion disks around a Schwarzschild black hole and a Kerr black hole with spin parameter $a = 0.998$ respectively. For the disk around a Schwarzschild black hole viewed at 45°, most photons from the first-order disk image that reach the observer have pitching angles very different from 45°. Moreover, a very substantial fraction of these photons leave the disk at very small pitching angles. Even at very high viewing angles (e.g. 85°), the fraction of small pitching-angle photons non-negligible. The variation in the pitching angles of photons across the accretion disk is more obvious for Kerr black holes. Photons from accretion disks around Kerr black holes are strongly lensed, and as in the case of the Schwarzschild black hole, the pitching angles of the photons that reach the observer are very different to the disk viewing inclination angle. Rotational frame-dragging effects are important. As shown in Figure 3 rotational frame dragging effects are very noticeable in the inner disk regions at a moderate disk viewing inclination angle (45°) as well as at a very high disk viewing inclination angle (85°).

We note rotational frame dragging has stronger effects on the pitching angles than the energy shifts of the photons. The reflection continuum, which is anisotropic, is thus more sensitive to the black hole's rotation than the lines, which depend on the black-hole spin parameter via a constraint on the inner radius of the accretion disk.

2.3 Spectral convolution

The spectral convolution calculations requires local reflection spectra with a range of photon pitching angles as imput, but XSPEC only generates spectra at fixed viewing angles. We therefore produce grids of spectra for a range of μ and interpolate between the grids for any arbitrary value of μ. We consider the Neville's algorithm (Press et al. 1992) for $n-$th order polynomial interpolation. The key features in the reflection spectra are the edges, otherwise the spectra consist of piecewise smooth curves (see Fig. 1). As a compromise between the two extremes, we use 5-th order polynomials in the spectral interpolations.

The emissions from each disk element are associated with a value of g and μ. We shift the energy of the spectrum of each disk element according to the corresponding g value and rescale the intensity by the factor g^4. We then re-bin the spectra, as the energy grid-points of the shifted spectra are generally not aligned with each other.

Finally, we specify the weights (relative contribution) of the reflection emission from the disk elements. We consider a parametric model for the disk emissivity which takes a power-law form: $I(E_{\rm e}, r_{\rm e}) \propto r_{\rm e}^{-\gamma}$, where $I(E_{\rm e})$ is the emitted intensity at energy $E_{\rm e}$, $r_{\rm e}$ is the radial distance of the emitting disk element from the central black hole, and γ is the power-law index. Summing all these weighted 'corrected' reflection spectra from the disk surface elements give the total spectrum of the accretion disk.

2.4 Basic parameters and other computational settings

We define a set of basic parameters (Table 1). Unless otherwise stated, we use this set of parameters in our calculations. The resolution of the disk images is chosen to be 250 × 250 pixels, sufficient to suppress the

Table 1: Basic set of system parameters used in the calculations

black-hole spin parameter, a	0.0
Inner disk radius, $r_{\rm in}$	$6\,r_{\rm g}$
Outer disk radius, $r_{\rm out}$	$20\,r_{\rm g}$
disk inclination angle, i	45°
Emissivity power-law index, γ	3
Incident photon index, Γ	1.7
Spectral cutoff energy, $E_{\rm c}$	150 keV
Metal abundance (relative to solar)	1.0
Iron abundance (relative to solar)	1.0
Spectral normalisation	1.0

numerical noise in the computation. The direct disk image and 2 next higher-order lensed images were included. For the grids of reflection rest-frame spectra generated by XSPEC, we set the grid step $\Delta\mu = 0.05$, in the range $0.05 < \mu < 0.95$. The energy range of the spectra is from 0.1 keV to 200 keV.

3 Results

The main features in a reflection rest-frame spectrum are the sharp C, O and Fe absorption edges. These edges are shifted and smeared in the reflection spectra due to gravitational lensing and various relativistic effects (cf. the spectra in the top panel of Fig. 4, see also the quotient spectrum of the relativistic case in the bottom panel). Note that the entire spectrum is red-shifted, and the effect is more visible at the high-energy (>10 keV) part of the spectrum. The energy shift is less apparent at the low- and medium-energies due to the profusion of spectral features.

In the following subsections, we will elaborate and assess how the relativistic reflection spectra are dependent on the system parameters. We consider a basic reference case with the parameters listed in Table 1, and unless otherwise stated we vary only one parameter at a time. We examined the effects of the disk inner radius $r_{\rm in}$, disk outer radius $r_{\rm out}$, disk emissivity profile power-law index γ, black-hole spin parameter a and disk viewing inclination angle i.

3.1 Inner disk radius

We begin by investigating the effects of the inner edge $r_{\rm in}$ of the accretion disk. We considered disks around non-rotating black holes (with $a = 0$). The outer disk radius is fixed, with $r_{\rm out} = 100\ r_{\rm g}$ but the inner radius is the parameter to vary. ($r_{\rm g} = GM/c^2$ is the gravitational radius, where M is the black-hole mass and c is the speed of light.) Figure 5 shows spectra for three values of the inner radius, $r_{\rm in} = 6$, 10 and 25 $r_{\rm g}$, (top panel) and the corresponding quotient spectra (bottom panel). As shown, the brightness of the disk reflection is dependent on the inner disk radius $r_{\rm in}$: the total intensity is larger for smaller $r_{\rm in}$. This can be explained by the fact that, when $r_{\rm out}$ is fixed, the total disk surface area is determined by $r_{\rm in}$. The differences between

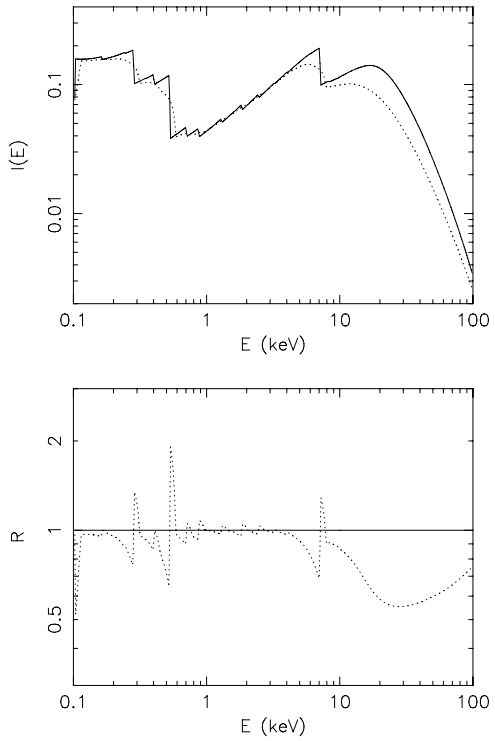

Figure 4: (Top) A reflection spectrum of a relativistic accretion disk around a Schwarzschild black hole (dotted line) in comparison to a reflection rest-frame MZ95 spectrum at a viewing angle of $\theta = 45°$. The intensities of the spectra $I(E)$ are in arbitrary units. (Bottom) The quotient spectra obtained by dividing the spectra by the reflection rest-frame spectrum. The normalisation is such that the normalised intensity $R = 1$ at the energy $E = 1$ keV in both cases.

the three spectra are manifested in the quotient spectra. The spiky features in the quotient spectra are due to the difference in the smearing and relative energy shifts of the edges, The difference between the spectra for $r_{\rm in} = 6$ and 10 $r_{\rm g}$ is smaller than the difference between the spectra for $r_{\rm in} = 6$ and 25 $r_{\rm g}$, indicative of importance of the relativistic effects in the inner region of the accretion disk. At energies above 10 keV, the quotient spectra show a broad 'dip' shape feature, which is a result of competition between energy-shift and smearing as well as lensing of the emission at the high-energy tails of the reflection rest-frame spectra from the disk surface elements.

3.2 Outer disk radius

For large values of the power-law index γ of the radial emissivity profile, the contribution to the spectrum is dominated by the inner disk region. We therefore choose a disk emissivity power-law law with $\gamma = 1$ (in-

Table 2: Radius of the last stable particle orbit, $r_{\rm ms}$, as a function of the black-hole spin parameter a.

a	$r_{\rm ms}/r_{\rm g}$
0.0	6.00
0.5	4.23
0.998	1.23

stead of 3 as in other cases) so to increase the relative contributions from the disk elements in the outer disk regions.

Figure 6 shows three reflection spectra and quotient spectra with $r_{\rm out}$ = 20, 50 and 100 $r_{\rm g}$. There is less overall emission from the disk with $r_{\rm out}$ = 20 $r_{\rm g}$, again for the reason that it has a smaller disk surface area. There are differences in the three spectra, mostly around the regions of the C, O and Fe features at ≈ 0.3, 0.6 and 7 keV. The spike and trough features are similar in the quotient spectra, which contrasts with the case of the variable $r_{\rm in}$ (cf. Fig. 6 and Fig, 5). The broad dip feature at energies above 10 keV is clearly visible in the quotient spectra. Here, it shows that adjusting $r_{\rm out}$ changes the relative contribution from the outer disk regions. In a large disk with a flat emissivity profile (small γ), the emission from the outer disk regions tend to overwhelm the strongly relativistically modified emissions from the inner disk regions.

3.3 Disk emissivity power-law index

The relative contributions of the inner and outer disk regions to the spectrum of an accretion disk are determined by the emissivity power-law index γ. Figure 7 shows the spectra and quotient spectra for γ = 1, 2 and 3. The total intensity of the reflection spectrum decreases as γ increases, while the differences between the overall shapes of the spectra are in the edges. The O and Fe edges become slightly less prominent when γ decreases, due to the fact that a small γ allows more reflection to come from the outer regions of the disk, which are less affected by the relativistic smearing and energy shifting. Note that the broad dip feature is present in the quotient spectra.

3.4 Spin of the black hole

Here, we set the inner rim of an accretion disk equal to the radius of last stable particle orbit, $r_{\rm ms}$. This is essentially to assume of a zero-torque boundary condition at the inner disk rim (Page & Thorne 1974; Eardley & Lightman 1975). As the last stable particle orbit $r_{\rm ms}$ is determined by the black-hole spin parameter a only, once we have specified a, $r_{\rm ms}$ is also determined. Table 2 shows the value of $r_{\rm ms}$ for three cases considered in our calculations (with a = 0, 0.5 and 0.998, corresponding to a Schwarzschild black hole, a modestly rotating Kerr black hole and a nearly extremal Kerr black hole).

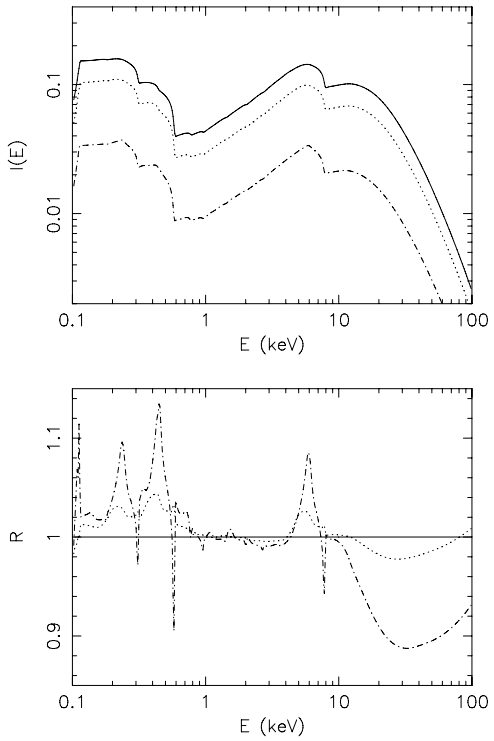

Figure 5: Spectra showing the effects due to changes in the inner radius of the accretion disk, $r_{\rm in}$. The top panel shows the reflection spectra of relativistic accretion disks with $r_{\rm in}$ = 6, 10 and 25 $r_{\rm g}$ (denoted by solid, dotted and dot-dashed lines respectively). The intensity $I(E)$ is in arbitrary units. The bottom panel shows the corresponding quotient spectra. The reflection spectrum of the case with $r_{\rm in}$ = 6 $r_{\rm g}$ is used as the reference spectrum to derive the quotient spectra. The normalisation is the same as in Fig. 4.

The spin of the black hole is an important parameter in determining the accretion disk reflection spectrum. An increase in the black-hole spin parameter a increases the total surface area of the accretion disk, if the outer disk radius is fixed. An immediate consequence is that this will increase the total intensity of the disk emissions. Another consequence is that this will increase the relative weight of the gravitationally shifted and lensed emissions from the innermost disk regions closed to the black-hole event horizon, in comparison to the emissions from the outer disk regions. In addition, the spin of the black hole determines the degree of rotational frame dragging, which, as shown in §2.2, can alters the distribution of pitching angles of the photons seen by the observer in the accretion disk. In Figure 8 we show the reflection spectra for the black-hole spin parameters a = 0.0, 0.5 and 0.998. The C, O and Fe edges are shifted to lower energies as a increases. The spiky features that had been seen

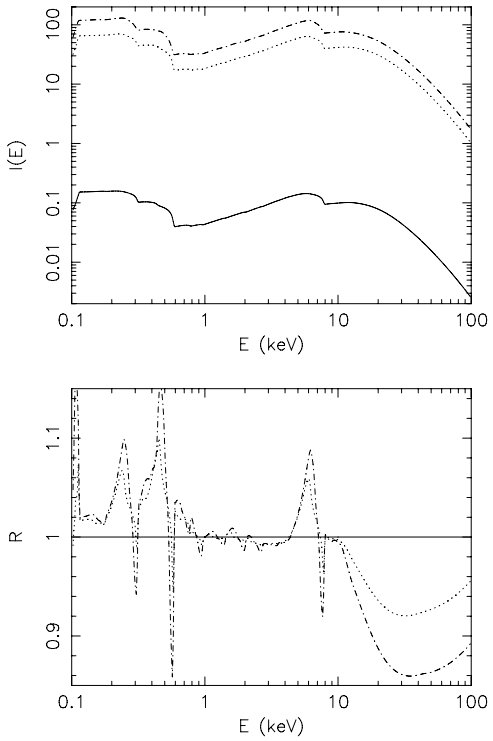

Figure 6: Same as Fig. 5 but for different disk outer radius $r_{\rm out}$. The reflection spectra and quotient spectra for $r_{\rm out}$ = 20, 50 and 100 $r_{\rm g}$. are denoted by solid, dotted and dot-dashed lines respectively. The emissivity profile is a power law with $\gamma = 1$. The case with $r_{\rm out} = 20\ r_{\rm g}$ is used as the reference spectrum to derive the quotient spectra.

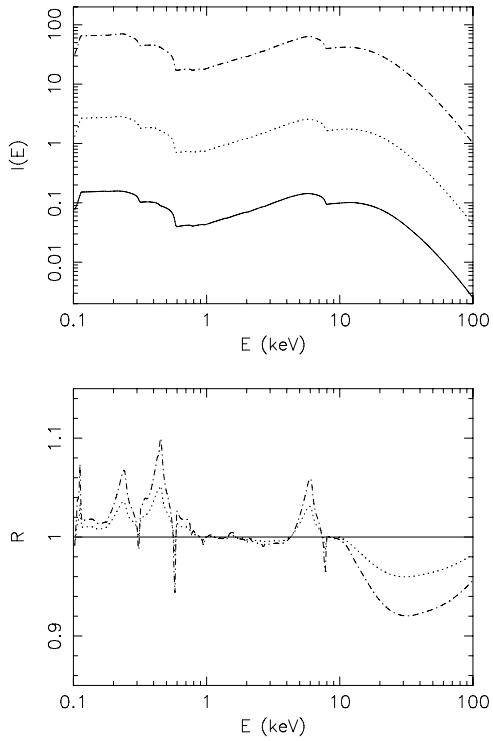

Figure 7: Same as Fig. 5 but for different disk emission power- law index γ. The curves in the top panel are the spectra for $\gamma = 3$, 2, and 1 (denoted by solid, dotted and dot-dashed lines respectively); the curves in the bottom panel are the corresponding quotient spectra, with respect to the case with $\gamma = 3$.

in the quotient spectra previously now become wedge-like, with an extensive low-energy (red) wing and a sharp higher-energy (blue) edge. The O and C wedges overlap substantially in the spectrum of $a = 0.998$. The dip feature at above 10 keV now disappears from the quotient spectrum.

3.5 Disk viewing inclination angle

Figure 9 shows the spectra for disks with $i = 1^\circ$, 45° and 85°. The intensity levels of the spectra of the disk with $i = 1^\circ$ and 45° are similar. This is as expected for the following reasons. At low inclination angles i the dominant effect is the time dilation (manifested as gravitational red-shift and transverse Doppler shift). Lensing is less important, as it does not increase the projected area of the disk substantially when i is small. The intensity is therefore still roughly proportional to $\cos i$, and the cosines of 1° and 45° differ by a factor less than unity. This proportionality no longer holds for larger inclination angles, because when i is sufficient large, gravitational lensing effect will be important. Nevertheless, even when the enhancement due to gravitational lensing and the additional contribution by the higher-order images are taken into account, the total intensities for the edge-on disks are smaller than the face-on disks provided that the index of the emissivity power law $\gamma \geq 2$ (cf. the spectra of the case with $i = 85^\circ$ and the other two in Fig. 9).

Figure 9 also demonstrates that relativistic effects are more important as i increases. The increases in the smearing of the edges can be seen when comparing the spectra for $i = 1^\circ$, 45° and 85°. Moreover, the spectra are shifted blue-ward when i increases, and the effects are more obvious in the quotient spectra. The increases in the blue shifts are due to the increase in the relativistic beaming/boosting and the decrease in the role of time dilation, as i increases. Note that the dip feature at energies above 10 keV that is seen in the quotient spectra in Figures 5, 6 and 7 is absent here.

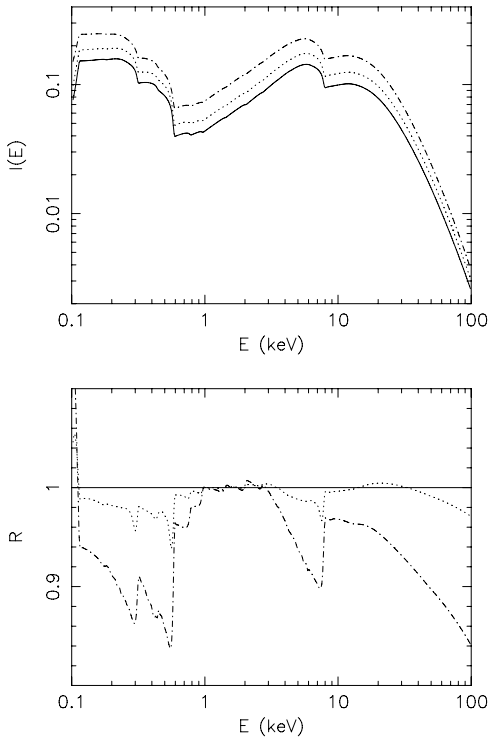

Figure 8: Same as Fig. 5 but for different values of black-hole spin parameter a. Spectra for $a = 0$, 0.5, and 0.998 (denoted by solid, dotted and dot-dashed lines respectively) are shown in the top panel and the corresponding quotient spectra, relative to the case $a = 0$, are shown in the bottom panel.

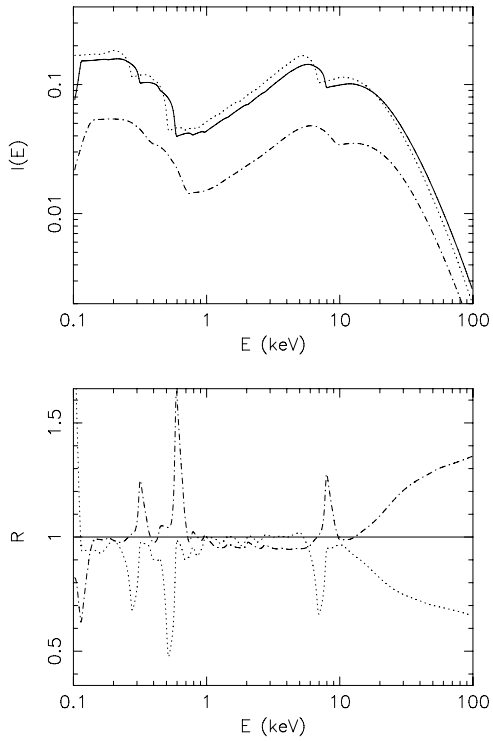

Figure 9: Same as Fig. 5 but for different disk inclination angles i. Spectra for $i = 1°$, 45° and 85° (denoted by dotted, solid and dot-dashed lines respectively) are shown in the top panel, and the corresponding quotient spectra, relative to the case $i = 45°$ are in the bottom panel.

4 Discussion and Conclusion

4.1 General aspects

Emissions from accretion disks around black holes can be substantially modified by various relativistic effects. The energies of the emissions are shifted and the intensities are boosted because of the high speeds of the accretion flows and because of time dilation resulting from the transverse motion of the emitters and the climbing of the deep gravitational well by the photons. The emissions can also be modified by gravitational lensing and rotational frame dragging. These two effects are particularly important if the emissions from the disk are anisotropic and have strong spatial dependence. Some of the relativistic effects have already been demonstrated in previous works on (isotropic) line profile calculations (e.g. Fabian et al. (1989); Fuerst & Wu (2004)). Here, we show the relativistic effects in the spectra of reflection emission of accretion disks, which is anisotropic and is subject to limb effects.

As the reflection continuum is angle dependent, it is more affected by gravitational lensing and the rotational frame-dragging than the isotropic line emission. In the absence of lensing, the observable emissions from a flat, thin disk are expected to have the same pitching angles as the disk viewing inclination angle i, implying that the direction of the 'observed' emissions from a disk with an almost edge-on viewing geometry should be almost aligned with the tangent of the disk surface emitting elements. We have shown that because of lensing, a substantial proportion of the observable emissions emerge at directions aligned close to the normals of the emitting disk surface elements even when the disk is viewed at an inclination angle $i = 85°$. Therefore, one cannot simply apply the energy shifts for the disk surface emitting elements and convolve with the corresponding local reflection rest-frame spectra. The angle-dependence must be considered explicitly, as in this work, when constructing the relativistic reflection model spectra.

We have assessed how the distortions of the reflection spectra depend on the system parameters. Careful examinations of the spectra and the quotient spectra reveal that certain effects are associated with some system parameters more than the others. The similarities between features in the quotient spectra in Figures 5, 6 and 7 are not all surprising, as the inner disk radius

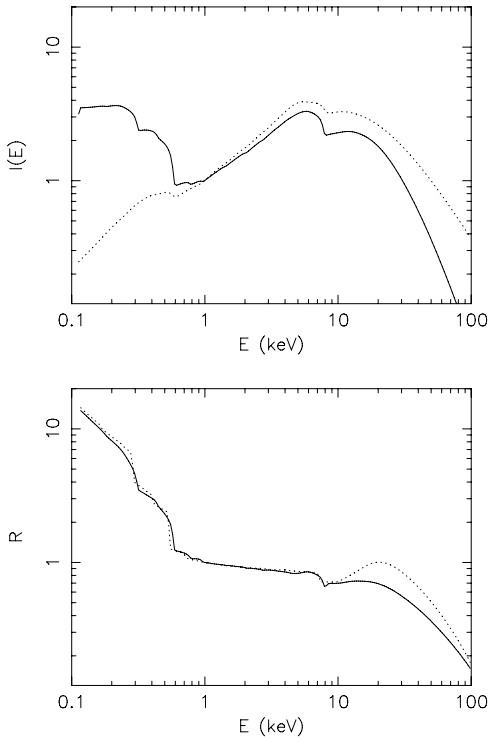

Figure 10: A comparison of relativistic reflection spectra (top panel) obtained by our convolution calculation (solid line) and by the DYK04 calculation (dotted line). A comparison of the ratio of the two spectra in the top panel (solid line) and the ratio of the PEXRAV spectrum and the HREFL spectrum (dotted line) (bottom panel). The viewing inclinations in both case are 45° and the spin-paramter of the black hole is 0. The other parameters are default as in Table 1. The normalisations are such that $I(E) = 1$ and $R = 1$ at $E = 1$ keV.

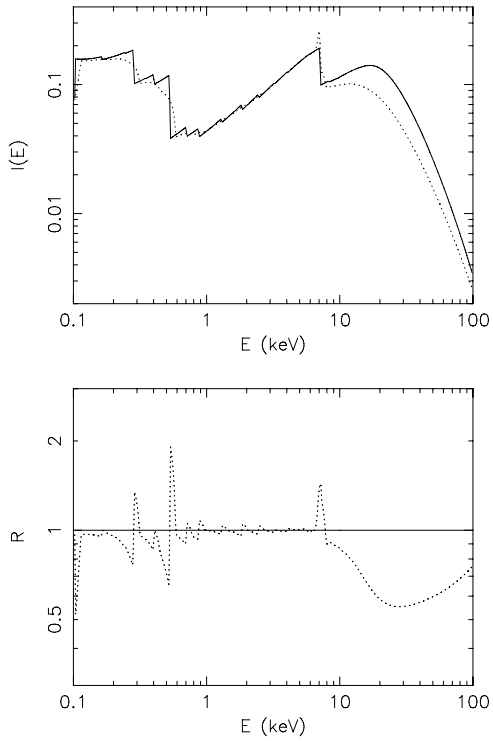

Figure 11: Same as Fig. 4, but a Fe Kα line at 6.4 keV is added to the relativistically modified reflection spectrum and the corresponding quotient spectrum.

$r_{\rm in}$, outer disk radius $r_{\rm out}$ and the emissivity power-law index γ have similar roles. They determine the relative contributions of emission by the disk surface elements. Adjusting them changes the weights of emission from the inner disk regions relative to the outer disk regions. In contrast, the smearing and energy shifts in the spectra in Figure 8 are different from those in the spectra in Figures 5, 6 and 7. The difference is more obvious in the corresponding quotient spectra. Here in this work, we have set the inner disk radius to be the last stable particle orbit which depends on the spin of the black hole only. The spin parameter a therefore uniquely determines how close the inner disk boundary can extend towards the black-hole event horizon. In the disk regions close to the black-hole event horizon, time dilation is the dominant effect and it always red-shifts the energies of the emissions. The wedge-like features in the quotient spectra in Figure 8 manifest the presence of large differential time dilation. The disk viewing inclination angle i is, however, more effective in causing energy shifting than smearing (cf. the quotient spectra in Fig. 9 and 8). This is due to the fact that the projected line-of-sight velocity is determined by i (except at very small radii, $r \ll 6\ r_{\rm g}$), and hence the main effect is relativistic Doppler shift. At large inclination angles, the 'blue' emissions are strongly boosted. We can may see blue-shifted features near the edges in the quotient spectrum of the case $i = 85°$ (Fig. 9). This is in contrast with that in the case of the black-hole spin, where the features are always red-shifted. Moreover, the smearing is smaller, because differential time dilation (due to gravitational red-shift) across the strongly emitting regions is relatively small, under the prescription that we have assumed for the inner disk boundary condition.

4.2 Comparison with other calculations

Calculations of relativistic reflection spectra have been carried out by various groups. Two representative calculations are Martoochia, Karas & Matt (2000) and Dovciak, Karas & Yaqoob (2004) (hereafter DKY04). The numerical algorithm used in the convolution calculations of this study is similar to that in DKY04.

Our results and the result of DKY04 are in qualitative agreement. However, a more careful examination reveals some subtle differences between the two calculations. These differences are sufficient to give rise to complications in spectral analysis and may cause further dispute in the interpretations of relativistic features in the X-ray spectra of AGN.

We have used the PEXRAV model to generate the input rest-frame reflection spectra, while DYK04 used the HREFL model. In the $1-10$ keV range, the HREFL model, which is a reasonable approximation, is a sensible choice (given that it takes much longer computation time to use the PEXRAV model to generate fine spectral grids). Outside the $1-10$ keV range, the two models differ very substantially. It is more desirable to consider the PEXRAV model for the input rest-frame spectral model. We show in Figure 10 (top panel) a relativistic reflection spectrum of an accretion disk around a Schwarzschild black hole viewed at an inclination of 45° and a relativistic reflection spectrum of the DYK04 model for the same parameters. The smeared and shifted metal edges in the relativistic spectrum below 0.5 keV are practically absent in the DYK04 spectrum. This is expected, as these edges are not obvious the HREFL model in the rest frame, in contrast to the PEXRAV model, where the edge features at these energies are prominent. While these relativistic edges may be ignored if we consider only a narrow spectral regions near the Fe Kα lines, a proper treatment of the edges below 0.5 keV is essential in the analysis of soft X-ray relativistic features, such as those seen in the *XMM-Newton* RGS spectra (see e.g. Branduardi-Raymont et al. (2001)).

The different input reflection rest-frame spectra explains part of but not all the differences between the relativistic reflection spectra obtained this study and in DKY04. The relativistic kernel function in the convolution calculation also plays an important role. The kernel function used in DYK04 has taken into account two main relativistic effects: the relativistic energy shifts and lensing (a default for most relativistic calculations). Calculations in this work also consider these two effects. In addition, we use a full radiative transfer formulation which takes account of anisotropy and limb brightening/darkening of the emission. The anisotropic and limb effects are particularly important for emission from the inner disk regions close to the central black hole, when gravitational lensing and relativistic aberration are most severe. To illustrate these effects, we compare two quotient spectra: the ratio of the PEXRAV model spectrum and the HREFL model spectrum and the ratio of the corresponding relativistic reflection spectra. In the comparison we choose a moderate viewing inclination angle of 45°, so that the effects are not excessively exaggerated as in the cases where the disk is viewed near edge-on. If the anisotropic and limb effects are unimportant, the two spectral ratios should be similar at all energies. If they are not, the diskrepancies in the two spectral ratios would be obvious. We show in the bottom panel of Figure 10 the ratio of the two relativistic reflection spectra presented in the top panel and the ratio of the PEXRAV model spectrum and the HREFL model spectrum viewed at 45°. The two ratios are far from being identical. The difference between the two ratios is quite significant ($> 50\%$) at energies above 10 keV. In the analysis of observed AGN spectra, such differences could cause large uncertainties in determining the underlying continuum, which needs to be subtracted in the fitting of the relativistic Fe Kα line. The difference between the two ratios is less obvious at lower energies but still visible. In particular, the location of the edges are different, causing by weighting differences when anisotropy and limb effects are present. This comparison also demonstrates that anisotropy and limb effects may distort the relativistic energy shifts of the edges, mimicking and partially masking the gravitational effects.

4.3 The presence of fluorescent emission lines

So far we have considered only the reflection spectra modified by relativistic effects and compared them with the reflection rest-frame spectra. In more realistic situations, the reflection continuum is often accompanied by lines. The lines, which also originate from the inner accretion disk region, are subject to relativistic effects. Figure 11 shows a spectrum consisting of a Fe Kα line and a reflection continuum component and its corresponding quotient spectrum. (The line is not included in the rest-frame model spectrum to illustrate the combined effects of shift/smearing of the edges and the presence of a relativistic line.) The inclusion of the line causes complication. This simple example demonstrates that the relativistic shifted red wing of the Fe line can 'fill up' its corresponding reflection edge. It is therefore a non-trivial task to separate the lines from the reflection continuum in an observed X-ray spectrum of AGN (especially in noisy low-resolution data) when both the components are severely shifted and smeared by various relativistic effects.

4.4 Summary

We have convolved angle-dependent rest-frame reflection spectra of accretion disks with relativistic ray-tracing radiative transfer calculations to generate relativistically modified reflection model spectra of accretion disks in AGN. We have shown that the resultant spectra are significantly modified, with edge smearing and energy shifting. The degrees of edge smearing and energy shifting depend on the accretion disk parameters as well as the black-hole spin. The smearing of the edges has strong dependence on the accretion disk outer and inner radii, the black-hole spin, and the disk emissivity profile. Energy shifting is, however, more affected by the accretion disk viewing inclination angle. Anisotropy and limb effects can sometimes mimick and partially mask the gravitational effects. These factors complicate the interpretation of X-ray spectral observations of AGN, as it is not straightforward to disentangle the effects on the lines, the edges and the underlying multi-component continuum of a severely relativistically modified AGN spectra.

Acknowledgments

KGL, GBR and KW acknowledge the support from the Nuffield Foundation through a Research Bursary program.

References

Branduardi-Raymont G., Sako M., Kahn S.M., Brinkman A.C., Kaastra J.S., Page M.J., 2001, A&A, 365, L140

Cunningham C.T., 1976, ApJ, 208, 788

Dabrowski Y., Fabian A.C., Iwasawa K., Lasenby A.N., Reynolds C.S., 1997, MNRAS, 288, L11

Dovciak M., Karas V., Yaqoob T., 2004, ApJS, 153, 205

Eardley D.M., Lightman A.M., 1975, ApJ, 200, 187

Fabian A.C., Rees M.J., Stella L., White N.E., 1989, MNRAS, 238, 729

Fanton C., Calvani M., De Felice F., Cadez A., 1997, PASJ, 49, 159

Fuerst S.V., 2005, PhD Thesis, University College London, University of London

Fuerst S.V., Wu K., 2004, A&A, 424, 733.

Magdziarz P., Zdziarski A.A., 1995, MNRAS 273 837

Martocchia A.,, Karas V., Matt G., 2000, MNRAS, 312, 817

Laor A., 1991, ApJ, 376, 90

Page D.N., Thorne K.S., 1974, ApJ, 191, 499

Pariev V.I., Bromley B.C., 1998, ApJ, 508, 590

Pozdnyakov L.A., Sobel I.M., Sunyaev R.A., 1983, Astron. and Sp. Phys. Rev., 2, 189

Press W.H., Teukolsky S.A., Vetterling W.T., Flannery B.P., 1992, Numerical Recipes in Fortran 77, 2nd Ed., Cambridge Univ. Press, Cambridge

Reynolds C.S., Nowak M.A., 2003, Phys. Reports, 377, 389

Reynolds C.S., Young A.J., Begelman M.C., Fabian A.C., 1999, ApJ, 514, 164

Shafer R.A., Haberl F., Arnaud K.A., 1991, XSPEC: An X-ray spectral fitting package, ESA TM-09, ESA, Paris

Stella L., 1990, Nature, 344, 747

Sunyaev R.A., Titarchuk L.G., 1980, A&A, 86, 121

Thorne K.S., Price R.H., 1975, ApJ, 195, L101

Wu K., Fuerst S.V., Lee K.-G., Branduardi-Raymont G., 2006, ChJAS, 6, 205